

Supporting Information

Stabilizing Cu⁺ species by Al-doping with enhanced *CO coverage for highly efficient electrochemical CO₂ reduction to C₂₊ products

Xuerong Wang, Qianqian Zhao, Shulin Zhao,* Aoshuang Pang, Luyao Yang, Yidan Sun, Yu Wang,* and Yuhui Chen*

X. Wang, Q. Zhao, S. Zhao, L. Yang, Y. Sun, Y. Chen

State Key Laboratory of Materials-Oriented Chemical Engineering, and School of Energy Science and Engineering, Nanjing Tech University, Nanjing 211816, China

E-mail: cheny@njtech.edu.cn

zhaosl@njtech.edu.cn

A. Pang, Y. Wang

Jiangsu Collaborative Innovation Centre of Biomedical Functional Materials, School of Chemistry and Materials Science, Nanjing Normal University, Nanjing 210023, China

E-mail: yu.wang@njnu.edu.cn

Experimental Details

Chemicals and materials

Copper nitrate trihydrate (AR) was bought from Aladdin Reagent Co., Aluminum nitrate trihydrate (AR), Sodium carbonate (AR), Sodium hydroxide (AR) was purchased from Sinopharm Chemical Reagent Company; Potassium hydroxide (>90%), Nafion (5 wt%) was obtained from Sigma-Aldrich; The water used in all the synthetic and catalytic performance measurement experiments was de-ionized (DI). All chemicals were used without further purification.

Preparation of the catalysts

In a typical synthesis of Cu₃Al-LDH nanosheets, the Cu(NO₃)₂·3H₂O (0.015 mol) and Al(NO₃)₃·9H₂O (0.005 mol) were dissolved in 18 mL of deionized water. The above solution was subsequently added to a stirred Na₂CO₃ solution (0.05 M). Then, the pH of the reaction system was maintained at ~9.5 by drop-wise addition of 1.5 M NaOH solution. The resulting blue suspension was aged 12 hours in a constant temperature water bath. Wash with deionized water several times until the pH of the supernatant is neutral, the product was freeze-dried to obtain Cu₃Al-LDHs for use. Moreover, by adjusting the ratio of Cu and Al salts to 1:1, 2:1, and 4:1, the Cu_xAl-LDHs with different Cu/Al ratios were obtained, labeled CuAl-LDHs, Cu₂Al-LDHs and Cu₄Al-LDHs, respectively.

For the Cu-LDHs, only Cu(NO₃)₂·3H₂O needs to be added to the synthesis system, and other experimental conditions are the same.

Material characterizations

Powder X-ray diffraction (XRD) data was collected using a Philips X'Pert PRO SUPER X-ray diffractometer equipped with graphite monochromatized Cu K α radiation ($\lambda=1.54056$ Å). The scanning electron microscopy (SEM) and transmission electron microscopy (TEM) characterizations were carried out using a HITACHI S-4800 and JEOL JEM-2100F operating at an acceleration voltage of 200 kV. High angle annular dark field scanning transmission electron microscopy (HAADF-STEM) and Energy dispersive X-ray spectroscopy (EDX) were carried out on JEOL JEM-2100F. X-ray photoelectron spectroscopy (XPS) measurements were performed on Thermo

Scientific K-Alpha using Al K α X-rays (1486.6 eV), where binding energies were calibrated by referencing the C1s peak (284.8 eV) to reduce the catalyst charge effect. The Cu and Al content were determined by an inductively coupled plasma optical emission spectrometer (ICP-OES, Thermo Fisher iCAP PRO).

Preparation of working electrodes

To prepare a working electrode, we dispersed 20 mg catalyst in a mixture of 4 mL isopropyl alcohol and deionized water, including 20 μ L Nafion solution (5 wt%), followed by ultrasonic for 20 minutes to obtain a uniform ink. Then, the catalyst ink was sprayed onto carbon paper with a gas diffusion layer and dried at 60 $^{\circ}$ C.

Electrochemical measurement

Electrochemical measurements were carried out in a typical flow cell consisting of a gas diffusion electrode (GDE) as the working electrode, Ni foam as the counter electrode, and Ag/AgCl (3 M KCl) as the reference electrode using a Biologic VMP3 multichannel potentiostat. All potentials were calibrated to the reversible hydrogen electrode (RHE) reference scale using E (V vs. RHE) = E (V vs. Ag/AgCl) + 0.059 \times pH + 0.205. A Nafion 115 proton exchange membrane separated the cathode liquid chamber from the anode chamber. The cathode and anode electrolyte were both 1.0 M KOH solution, and the liquid phase circulation was realized by a peristaltic pump. CO₂ gas was introduced as a reactant and the flow was controlled by a mass flowmeter. The working electrode and the opposite electrode were fixed with conductive copper tape.

To quantify each product, we performed CO₂ electrolysis by a chronopotentiometry mode. The gaseous products (such as H₂ and C₂H₄) were quantified using a gas chromatography (GC) system (Nanjing Hope, GC-9860-5C) that was equipped with a flame ionization detector (FID) and a thermal conductivity detector (TCD). Liquid products were analyzed by ¹H-nuclear magnetic resonance (¹H-NMR, Bruker AVANCE AV-300).

Faradaic efficiency (FE) of gas products can be calculated as follows:

$$FE_{gas}(\%) = \frac{n * F * v * P * f_i * A}{R * T * I} * 100\%$$

Where n is the number of electrons transferred to produce a product molecule; F is the Faradaic constant; v is the CO₂ gas flow (m³ s⁻¹); P is the ambient pressure (1.013 × 10⁵ Pa); f_i is the correction factor for gas product; A is the peak area corresponding to the gas product; R is the gas constant (8.314 J mol⁻¹ K⁻¹); T is the test temperature (298.15 K); I is the steady state cell current (A).

Liquid sample (0.5 mL) was collected at the end of each experiment, and was mixed with internal standard dimethyl sulfoxide (DMSO, Sigma 99.99%) in D₂O solution (0.1 mL 0.65 mM). The quantities of products were calculated by comparing the integral areas of an observed liquid product with that of the DMSO. The FE of liquid sample can be calculated by using the following equation:

$$FE_{liquid}(\%) = \frac{n * F * C_x * V_{cell}}{I * t} * 100\%$$

Where n is the number of electrons required for the liquid product; F is the Faradaic constant; C_x is the concentration of liquid product (mol L⁻¹); V is the electrolyte volume (L); I is the steady state battery current (A); t is the test time (s).

Double-layer capacitance (C_{dl}) measurements. C_{dl} was determined by measuring the capacitive current associated with double-layer charging from the scan-rate dependence of cyclic voltammogram (CV). The CV test was also performed in a flow cell, consistent with performance test conditions. The test range is 0.3 V - 0.4 V (vs. Ag/AgCl). C_{dl} was estimated by plotting $\Delta j (j_a - j_c)$ with the scanning rate at 0.35 V (vs. Ag/AgCl), where j_a and j_c are anode and cathode current densities, respectively. The scan rates are 20, 40, 60, 80, 100 and 120 mV s⁻¹, respectively.

Electrochemical impedance spectroscopy (EIS) measurements. The EIS measurements were performed on CHI 660E at a voltage of -1.5 V (vs. RHE), applying an AC voltage of 10 mV amplitude over a frequency range of 10⁶ Hz to 0.1 Hz.

In situ XRD measurements

The in situ XRD pattern was recorded by Smart-Lab diffractometer and self-made three-electrode electrochemical cell. Hydrophobic carbon paper coated with catalyst, Ag/AgCl (3 M KCl) electrode, and Ni foam corresponds to the working electrode, reference electrode, and reverse electrode respectively. CO₂-saturated 0.5 M KHCO₃

solution was used as the electrolyte. X-ray diffraction patterns are recorded in reflection mode (Bragg-Brentano geometry) with steps of $10^\circ \text{ min}^{-1}$ and 2θ values of 10° to 70° .

In situ Raman measurement

The in situ Raman studies were carried out on the Xplora Plus Raman spectrometer and a self-made three-electrode electrochemical flow cell, which is composed of carbon paper catalyst as working electrode, Ag/AgCl (3 M KCl) reference electrode and Ni foam counter electrode. The working electrode was prepared by coating $\text{Cu}_3\text{Al-LDHs}$ and Cu-LDHs catalyst drops on hydrophobic carbon paper. 1.0 M KOH solution was used as the electrolyte to pass CO_2 into the gas bin for collection during the test.

Computational methods

DFT calculations were performed in the Vienna Ab initio Software Package (VASP) using the projector-augmented plane wave (PAW) approach and Perdew-Burke-Ernzerhof (PBE) functional.^[1] A 400 eV cutoff energy for the plane wave expansion was adopted, and the k-space sampling was set as $4 \times 4 \times 1$. Convergence criteria of energy and force were set as $1 \times 10^{-5} \text{ eV}$ and 0.05 eV/\AA , respectively. Treating the van der Waals (vdW) interactions by Grimme's D3 dispersion method.^[2] According to a previous study, the GGA+U scheme ($U-J = 5.2 \text{ eV}$)^[3] introduced by Dudarev et al.^[4] was employed to describe the strongly correlated d electrons of Cu. The solvation effect was treated using the Poisson-Boltzmann implicit solvation model.^[5] The transition state (TS) was located using the climbing image nudged elastic band (CI-NEB) method and verified by vibrational frequency calculations (only one imaginary frequency).^[6]

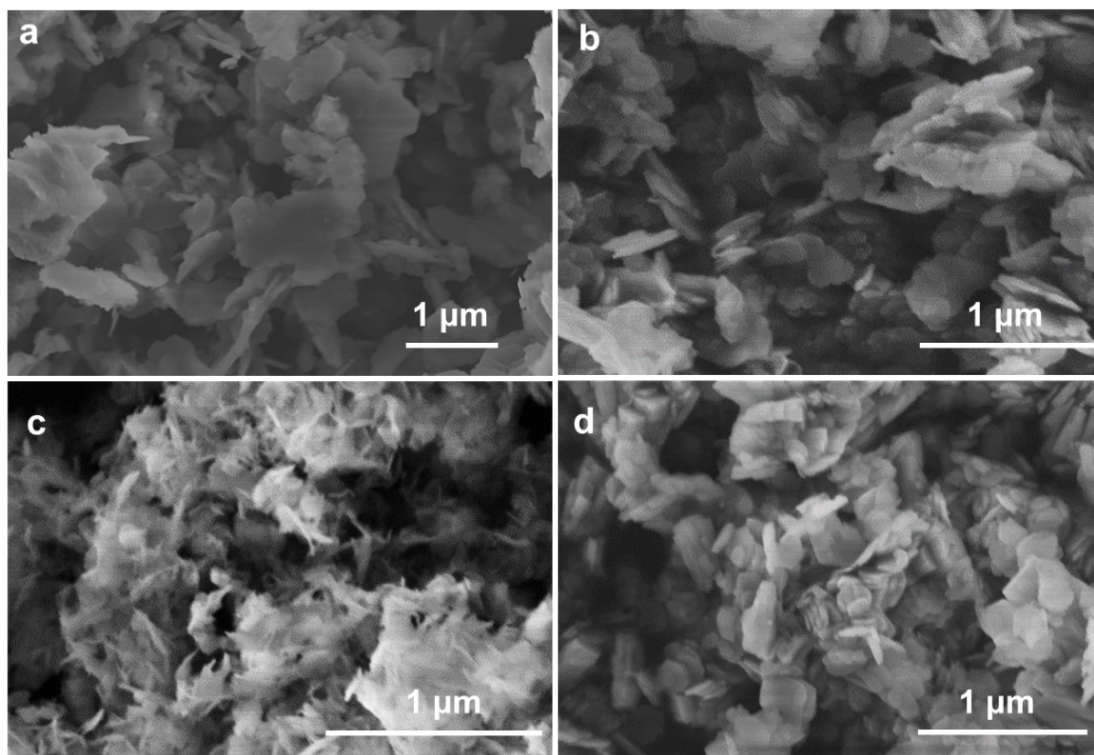


Figure S1. SEM images of (a) CuAl-LDHs, (b) Cu₂Al-LDHs, (c) Cu₃Al-LDHs, and (d) Cu₄Al-LDHs.

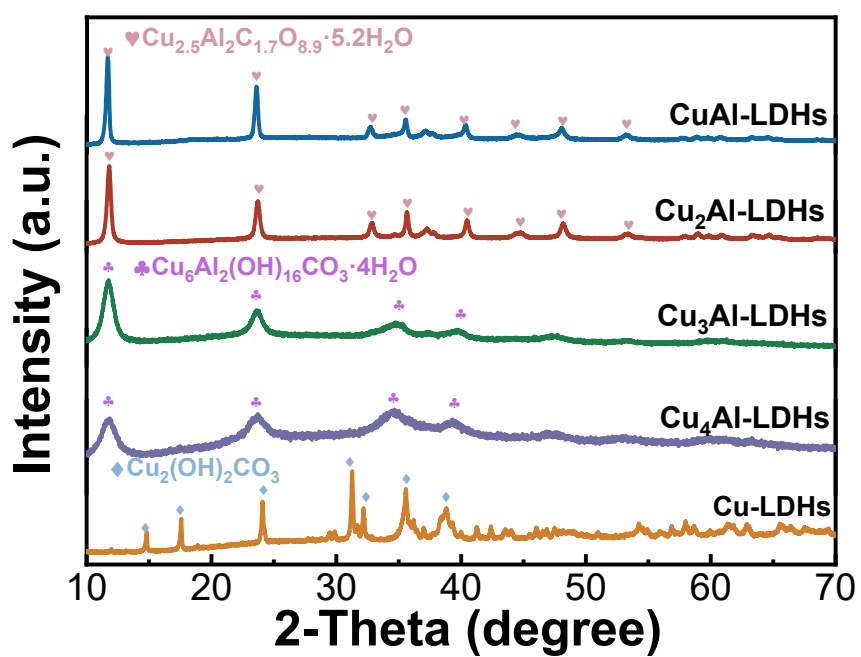


Figure S2. XRD patterns of the Cu_xAl-LDHs catalysts.

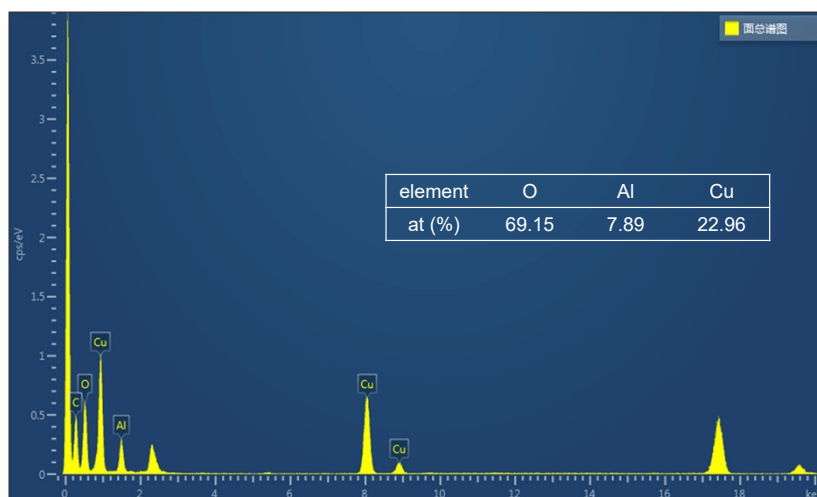


Figure S3. The EDX patterns of the obtained $\text{Cu}_3\text{Al-LDHs}$ catalysts.

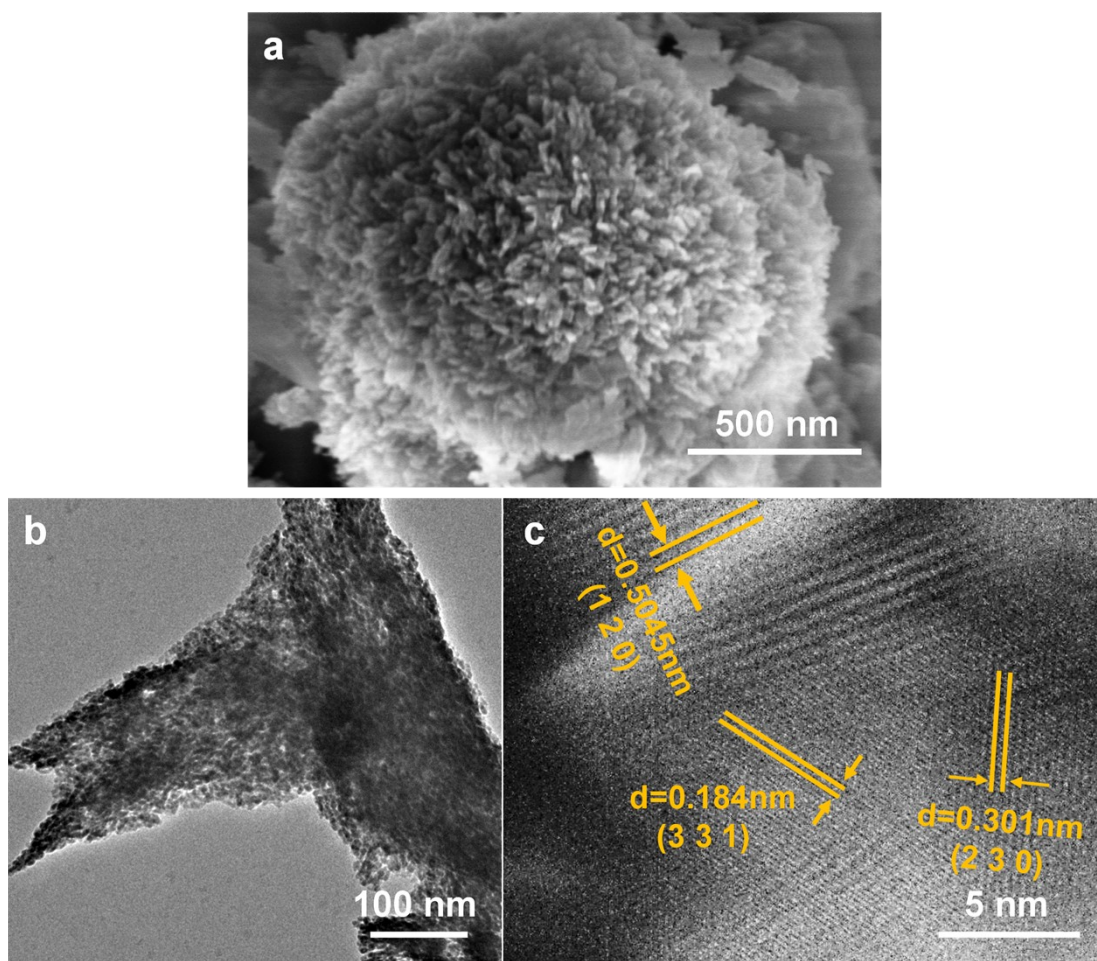


Figure S4. (a) SEM image, (b) TEM image, and (c) HRTEM of Cu-LDHs.

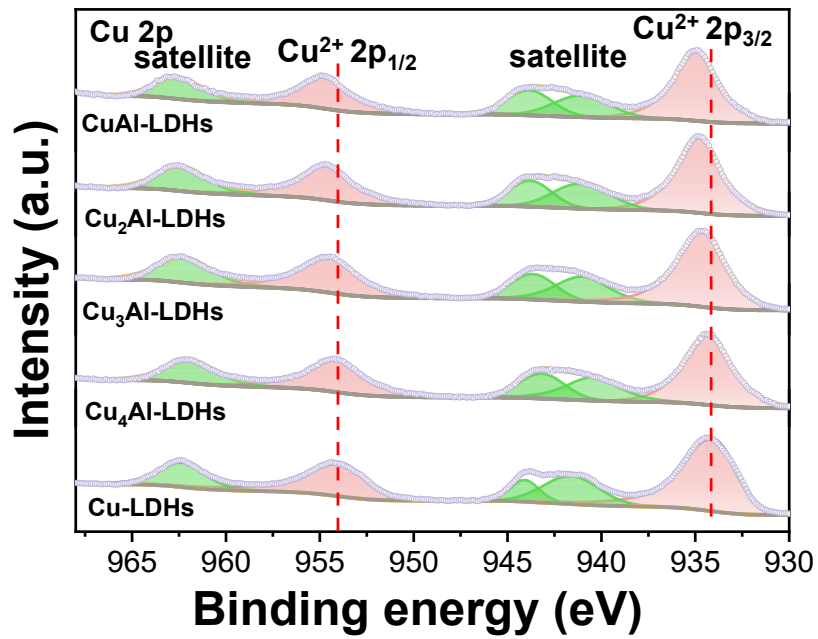


Figure S5. High-resolution XPS Cu 2p spectra of the Cu_xAl-LDHs catalysts.

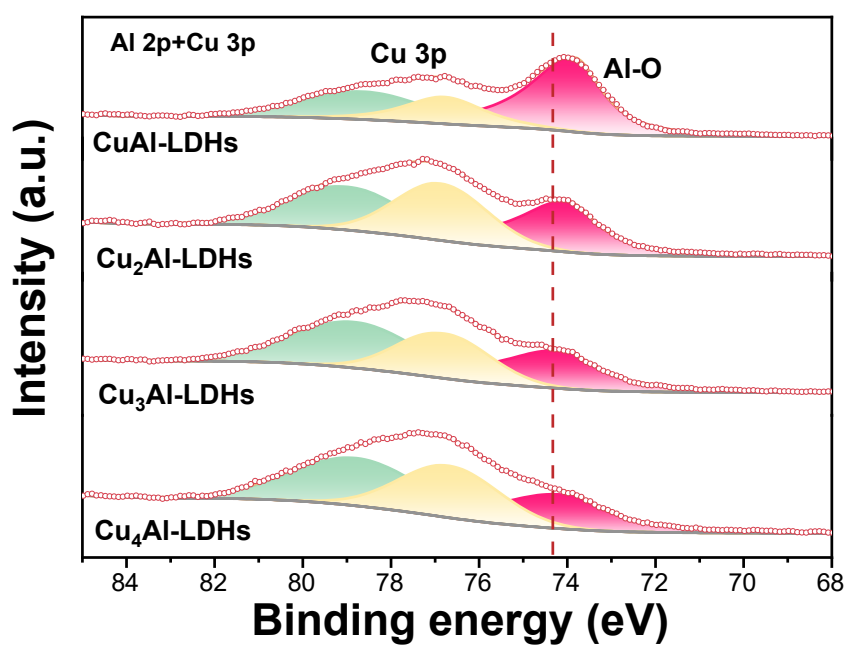


Figure S6. High-resolution XPS Al 2p+Cu 3p spectra of the Cu_xAl-LDHs catalysts.

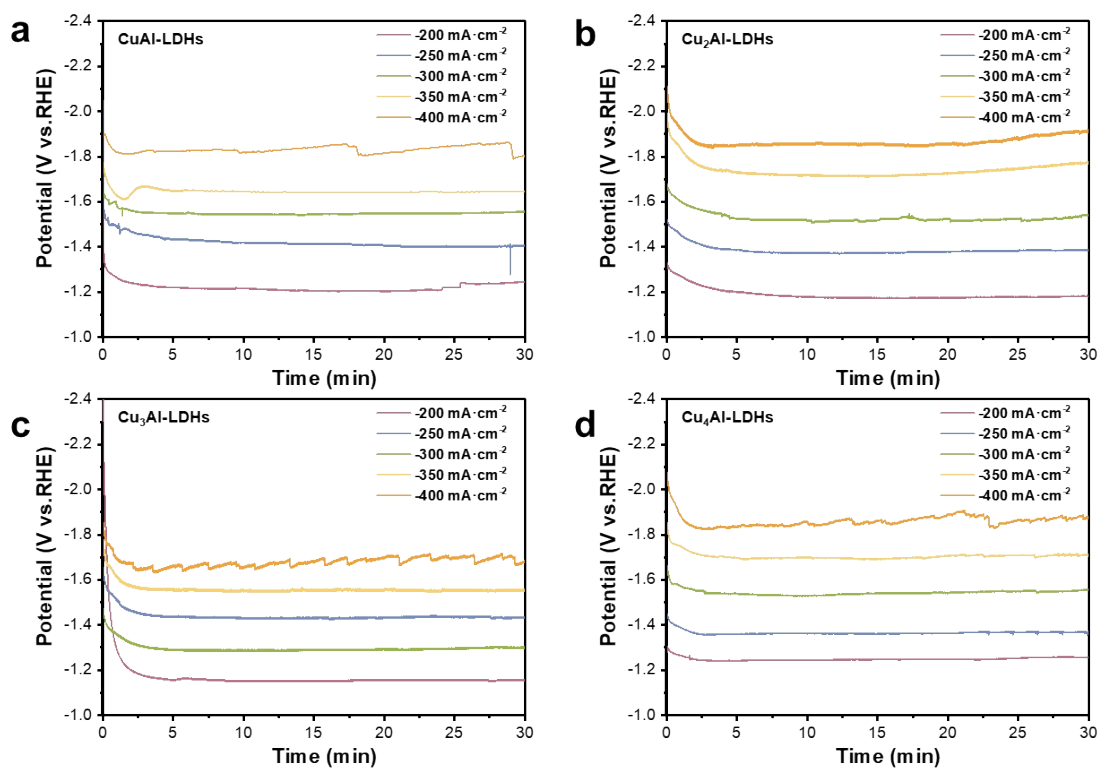


Figure S7. Chronoamperometric test curves for different catalysts. (a) CuAl-LDHs, (b) Cu₂Al-LDHs, (c) Cu₃Al-LDHs, and (d) Cu₄Al-LDHs.

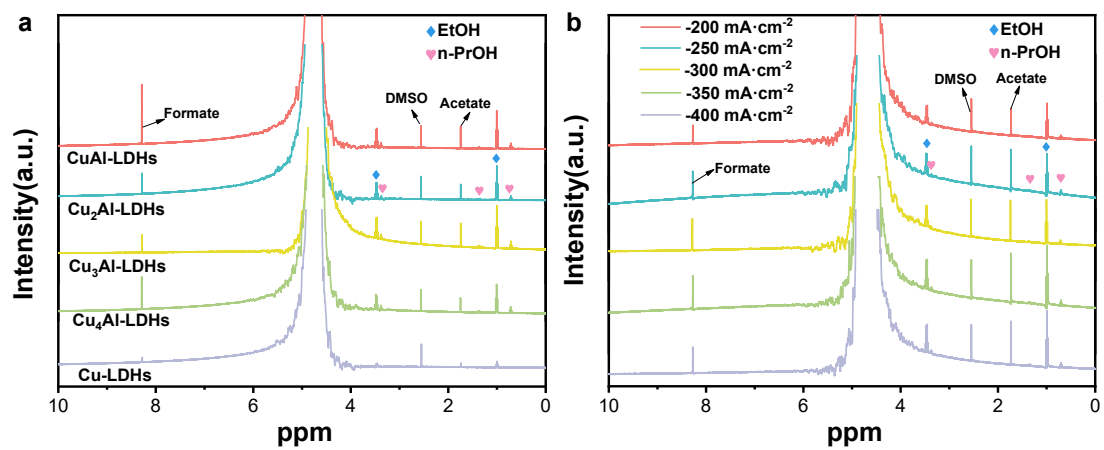


Figure S8. The ^1H NMR spectra of the electrolyte after the reduction of CO_2 from (a) different $\text{Cu}_x\text{Al-LDHs}$ and Cu-LDHs catalysts at a current density of $-300 \text{ mA}\cdot\text{cm}^{-2}$. (b) $\text{Cu}_3\text{Al-LDHs}$ at different current densities

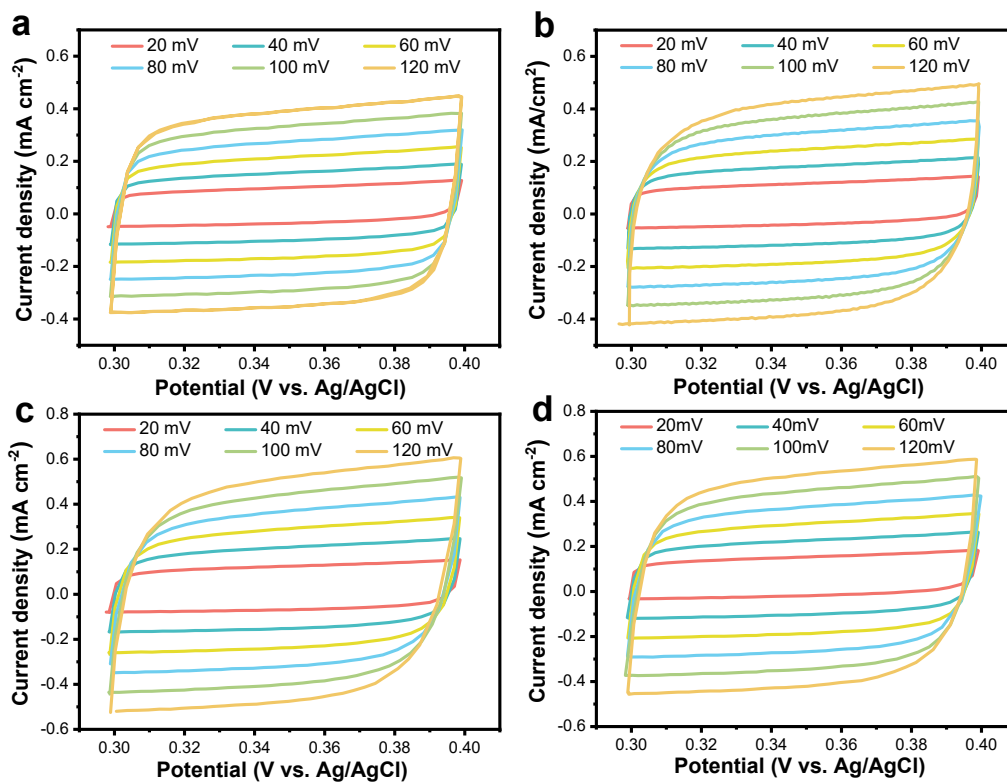


Figure S9. Cyclic voltammetry curves for (a) CuAl-LDHs, (b) Cu₂Al-LDHs, (c) Cu₃Al-LDHs, and (d) Cu₄Al-LDHs measured at 0.3-0.4 V (vs Ag/AgCl) with the scan rates ranging from 20 to 120 mV s⁻¹.

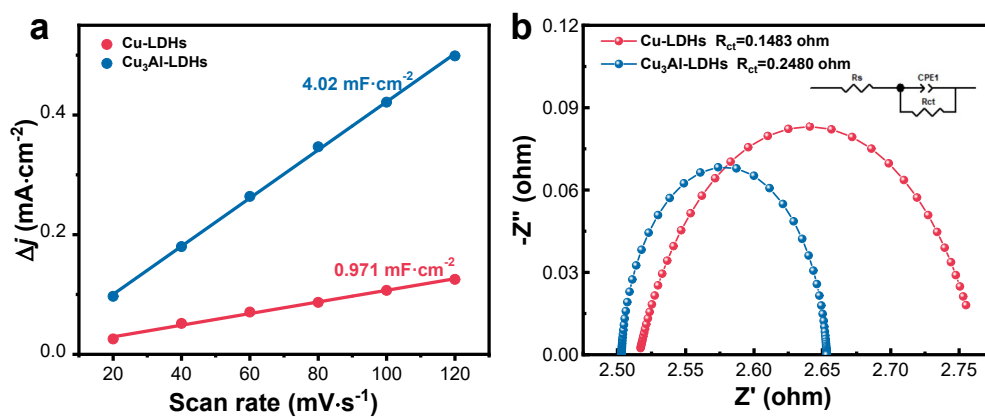


Figure S10. (a) Linear fitting of double-layer capacitive currents density as a function of the scan rate to estimate ECSA for Cu₃Al-LDHs and Cu-LDHs. (b) Nyquist plots (inset: equivalent circuit) of Cu₃Al-LDHs and Cu-LDHs.

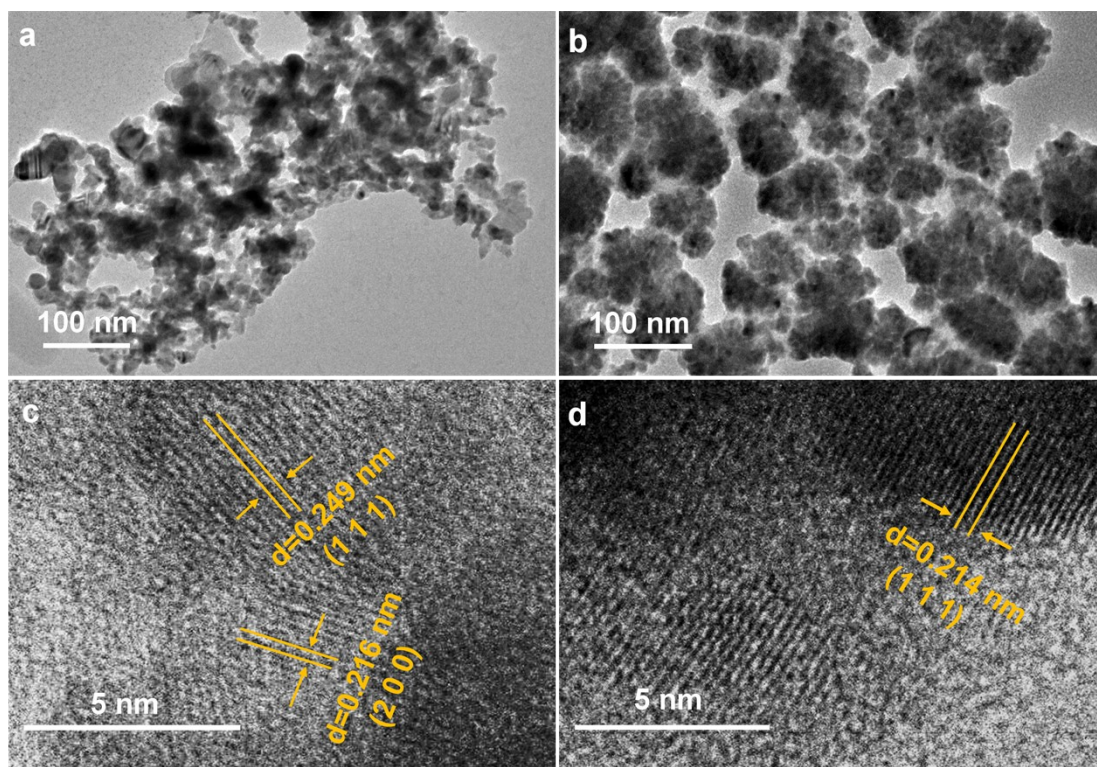


Figure S11. TEM images of (a) Cu₃Al-LDHs and (b) Cu-LDHs after CO₂RR test. HRTEM images of (c) Cu₃Al-LDHs and (d) Cu-LDHs after CO₂RR test.

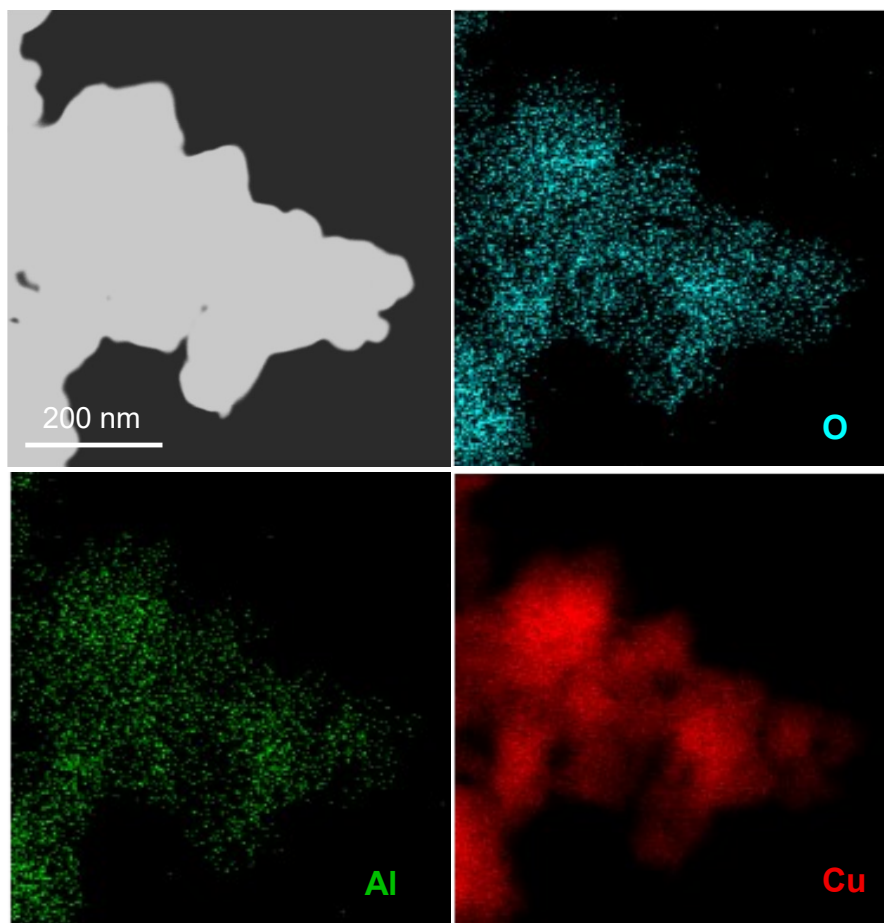


Figure S12. The HAADF-STEM image and corresponding EDX elemental mappings of Cu₃Al-LDHs after the CO₂RR test.

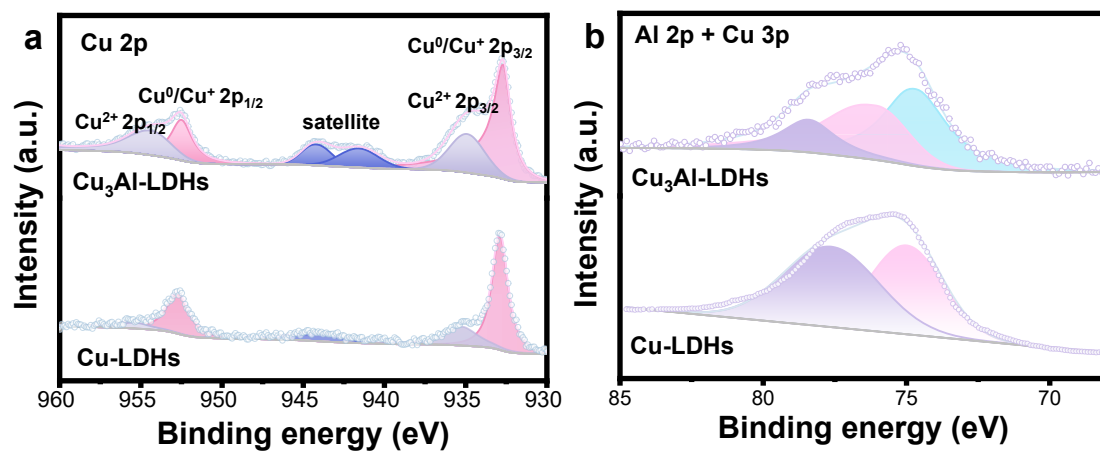


Figure S13. XPS high-resolution spectra of $\text{Cu}_3\text{Al-LDHs}$ and Cu-LDHs after CO_2RR test. (a) $\text{Cu } 2p$ and (b) $\text{Al } 2p + \text{Cu } 3p$.

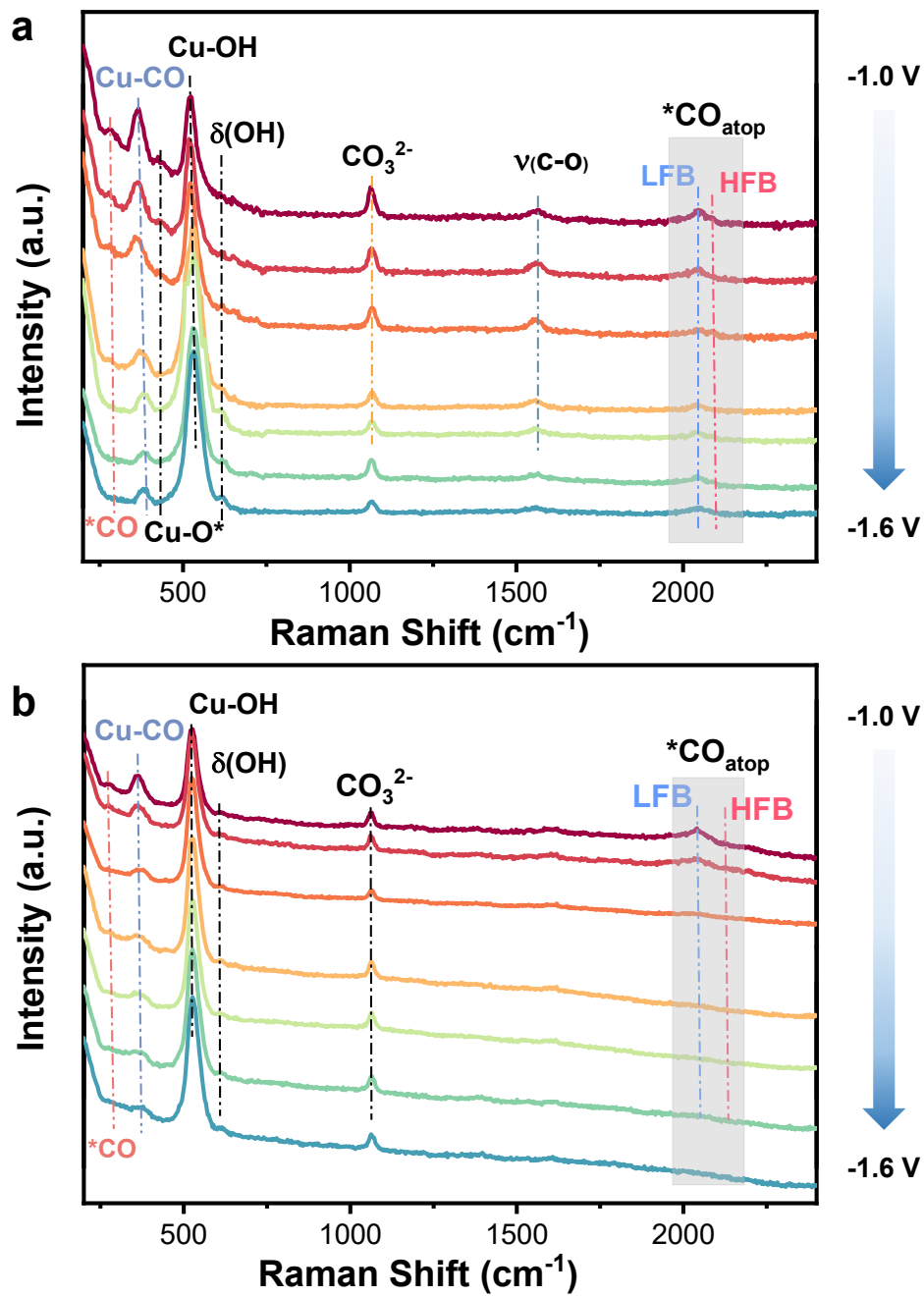


Figure S14. In situ Raman spectroscopy during CO₂RR. (a) Cu₃Al-LDHs and (b) Cu-LDHs.

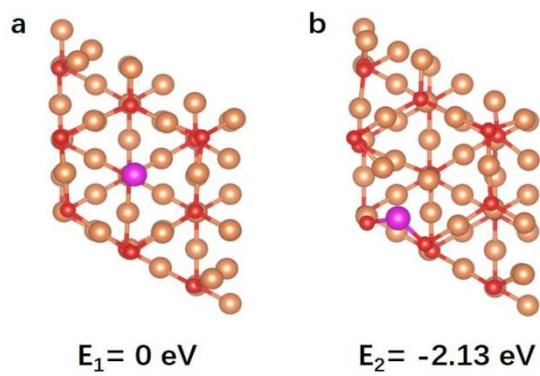


Figure S15. Top view of Cu₂O-Al with Al atom substituting (a) the Cu_A atom and (b) the Cu_B atom. The numbers indicate their relative energy.

Table S1. ICP-OES test results before CO₂RR and after CO₂RR for different catalysts

	Catalysts	n_{Cu}/n_{Al}
before CO ₂ RR	CuAl-LDHs	0.95
	Cu ₂ Al-LDHs	1.74
	Cu ₃ Al-LDHs	2.56
	Cu ₄ Al-LDHs	3.4
after CO ₂ RR	CuAl-LDHs-R	3.1
	Cu ₂ Al-LDHs-R	11.1
	Cu ₃ Al-LDHs-R	27.4
	Cu ₄ Al-LDHs-R	12.3

Table S2. Comparison of the $FE_{C_{2+}}$ and C_{2+} partial current densities of the Cu_3Al -LDHs catalyst with state-of-the-art Cu-based catalysts.

Catalyst	Electrolyte	$FE_{C_{2+}}$	$j_{C_{2+}}$	C_2/C_1	Ref
Cu_3Al LDHs	1M KOH	84.7%	252	9	This work
Cu LDHs	1M KOH	37.5%	112.5	1.31	work
N-Cu	1M KOH	73.7%	909	5.67	[7]
$Cu_2P_2O_7$	0.1 M KOH	73.6%	258	/	[8]
CuO-FEP	1 M KOH	77%	616	/	[9]
Reconstructed Cu	3M KOH	84%	336	/	[10]
NiOOH/Cu	1 M KOH	83.4%	417	13.1	[11]
hydroxyl-mediated OD-Cu	1 M $KHCO_3$	81.45	285.1	11.34	[12]
Gd_1/CuO_x	2 M KOH	81.4%	444.3	12	[13]
CuNWs-CoPc	1 M KOH	69.9%	104.8	13.98	[14]
CuO-BPNF	1 M KOH	74.7%	177.9	4.5	[15]
$La(OH)_3/Cu$	1 M KOH	71.2%	712.6	8.3	[16]
$CuO_x@C$	1 M KOH	82%	315	8	[17]
3-shell HoMSs	0.5 M $KHCO_3$	77%	514	6.5	[18]
Cu_3N_x -50- μA	1 M KOH	81.7	306	7.9	[19]
Cu_3Al MONFs	1 M KOH	76.4	458	9.7	[20]
Cu-CuI composite	1 M KOH	~70%	591	3.5	[21]
Defect-Site-Rich Cu	0.5 M $KHCO_3$	72%	72	3.8	[22]
NGQ/Cu nanorods	1 M KOH	80.4%	282	/	[23]
Cu-Ag	1 M KOH	~80%	160	/	[24]

References

- [1] a) G. Kresse, J. Hafner. *Phys. Rev. B.* **1993**, *47*, 558-561; b) J. P. Perdew, K. Burke, M. Ernzerhof. *Phys. Rev. Lett.* **1996**, *77*, 3865-3868; c) P. E. Blöchl. *Phys. Rev. B* **1994**, *50*, 17953-17979.
- [2] S. Grimme, S. Ehrlich, L. Goerigk. *J. Comput. Chem.* **2011**, *32*, 1456-1465.
- [3] K. Bhola, J. J. Varghese, L. Dapeng, Y. Liu, S. H. Mushrif. *J. Phys. Chem. C* **2017**, *121*, 21343-21353.
- [4] S. L. Dudarev, G. A. Botton, S. Y. Savrasov, C. J. Humphreys, A. P. Sutton. *Phys. Rev. B* **1998**, *57*, 1505-1509.
- [5] a) K. Mathew, R. Sundararaman, K. Letchworth-Weaver, T. A. Arias, R. G. Hennig. *J. Chem. Phys.* **2014**, *140*, 084106; b) K. Mathew, V. S. C. Kolluru, S. Mula, S. N. Steinmann, R. G. Hennig. *J. Chem. Phys.* **2019**, *151*, 234101.
- [6] G. Henkelman, B. P. Uberuaga, H. Jónsson. *J. Chem. Phys.* **2000**, *113*, 9901-9904.
- [7] M. Zheng, P. Wang, X. Zhi, K. Yang, Y. Jiao, J. Duan, Y. Zheng, S.-Z. Qiao. *J. Am. Chem. Soc.* **2022**, *144*, 14936-14944.
- [8] J. Sang, P. Wei, T. Liu, H. Lv, X. Ni, D. Gao, J. Zhang, H. Li, Y. Zang, F. Yang, Z. Liu, G. Wang, X. Bao. *Angew. Chem. Int. Ed.* **2021**, *61*, e202114238.
- [9] T. H. M. Pham, J. Zhang, M. Li, T. H. Shen, Y. Ko, V. Tileli, W. Luo, A. Züttel. *Adv. Energy Mater.* **2022**, *12*, 2103663.
- [10] M. G. Kibria, C. T. Dinh, A. Seifitokaldani, P. De Luna, T. Burdyny, R. Quintero-Bermudez, M. B. Ross, O. S. Bushuyev, F. P. García de Arquer, P. Yang, D. Sinton, E. H. Sargent. *Adv. Mater.* **2018**, *30*, 1804867.
- [11] X. Mao, C. W. Chang, Z. Li, Z. Han, J. Gao, M. Lyons, G. Sterbinsky, Y. Guo, B. Zhang, Y. Wang, X. Wang, D. Han, Q. H. Yang, Z. Feng, Z. Weng. *Adv. Energy Mater.* **2024**, 2400827.
- [12] C. Li, Z. Guo, Z. Liu, T. Zhang, H. Shi, J. Cui, M. Zhu, L. Zhang, H. Li, H. Li, C. Li. *ACS Catal.* **2023**, *13*, 16114-16125.
- [13] J. Feng, L. Wu, S. Liu, L. Xu, X. Song, L. Zhang, Q. Zhu, X. Kang, X. Sun, B. Han. *J. Am. Chem. Soc.* **2023**, *145*, 9857-9866.
- [14] Y. Luo, J. Yang, J. Qin, K. Miao, D. Xiang, A. Kuchkaev, D. Yakhvarov, C. Hu, X. Kang. *J. Energy Chem.* **2024**, *92*, 499-507.

- [15] F. Pan, X. Duan, L. Fang, H. Li, Z. Xu, Y. Wang, T. Wang, T. Li, Z. Duan, K. J. Chen. *Adv. Energy Mater.* **2023**, *14*, 2303118.
- [16] S. Hu, Y. Chen, Z. Zhang, S. Li, H. Liu, X. Kang, J. Liu, S. Ge, J. Wang, W. Lv, Z. Zeng, X. Zou, Q. Yu, B. Liu. *Small.* **2023**, *20*, 2308226.
- [17] Y. Zang, T. Liu, P. Wei, H. Li, Q. Wang, G. Wang, X. Bao. *Angew. Chem. Int. Ed.* **2022**, *61*, e202209629.
- [18] C. Liu, M. Zhang, J. Li, W. Xue, T. Zheng, C. Xia, J. Zeng. *Angew. Chem. Int. Ed.* **2021**, *61*, e202113498.
- [19] C. Peng, G. Luo, Z. Xu, S. Yan, J. Zhang, M. Chen, L. Qian, W. Wei, Q. Han, G. Zheng. *Adv. Mater.* **2021**, *33*, 2103150.
- [20] M. Fang, Y. Ji, Y. Pi, P. Wang, Z. Hu, J.-F. Lee, H. Pang, Y. Li, Q. Shao, X. Huang. *Chem. Mater.* **2022**, *34*, 9023-9030.
- [21] H. Li, T. Liu, P. Wei, L. Lin, D. Gao, G. Wang, X. Bao. *Angew. Chem. Int. Ed.* **2021**, *60*, 14329-14333.
- [22] Z. Gu, H. Shen, Z. Chen, Y. Yang, C. Yang, Y. Ji, Y. Wang, C. Zhu, J. Liu, J. Li, T.-K. Sham, X. Xu, G. Zheng. *Joule.* **2021**, *5*, 429-440.
- [23] C. Chen, X. Yan, S. Liu, Y. Wu, Q. Wan, X. Sun, Q. Zhu, H. Liu, J. Ma, L. Zheng, H. Wu, B. Han. *Angew. Chem. Int. Ed.* **2020**, *59*, 16459-16464.
- [24] C. Chen, Y. Li, S. Yu, S. Louisia, J. Jin, M. Li, M. B. Ross, P. Yang. *Joule.* **2020**, *4*, 1688-1699.